doi:10.1093/plphys/kiab002 PLANT PHYSIOLOGY 2021: 185: 1682–1696

Plant Physiology

Research Article

Declining carbohydrate content of Sitka-spruce treesdying from seawater exposure

Peipei Zhang,[1,2] Nate G. McDowell,[2,3,†], Xuhui Zhou ,[1,*,†] Wenzhi Wang,[2] Riley T. Leff,[2] Alexandria L. Pivovaroff ,[2] Hongxia Zhang ,[2] Pak S. Chow ,[4] Nicholas D. Ward,[5,6] Julia Indivero,[5] Steven B. Yabusaki ,[7] Scott Waichler [7] and Vanessa L. Bailey [8]

1 Center for Global Change and Ecological Forecasting, Shanghai Key Lab for Urban Ecological Processes and Eco-Restoration, School of Ecological and Environmental Sciences, East China Normal University, Shanghai 200241, China
2 Atmospheric Sciences & Global Change, Pacific Northwest National Laboratory, Richland, Washington 99354, USA
3 School of Biological Sciences, Washington State University, Pullman, Washington 99164-4236, USA
4 Department of Renewable Resources, University of Alberta, Edmonton, Alberta, Canada T6G 2R3
5 Marine Sciences Laboratory, Pacific Northwest National Laboratory, Sequim, Washington 98382, USA
6 School of Oceanography, University of Washington, Seattle, Washington 98195, USA
7 Earth Systems Science, Pacific Northwest National Laboratory, Richland, Washington 99354, USA
8 Biological Sciences Division, Pacific Northwest National Laboratory, Richland, Washington 99354, USA

*Author for communication: xhzhou@des.ecnu.edu.cn
†Senior authors.

N.G.M., P.Z., W.W., N.D.W., and V.L.B. contributed to the design of the research. N.G.M., P.Z., W.W., H.Z, and J.I. conducted the field work. P.Z. and R.T.L. performed carbohydrate analysis with guidance from P.S.K. P.Z., and N.G.M. A.L.P. contributed to data analysis and interpretation of results. S.Y. and S.W. performed the modeling of subsurface salinity. P.Z. took the lead in writing the article with contributions from N.G.M. and X.Z., and feedback and approval from all coauthors. N.G.M. and X.Z. agree to serve as the authors responsible for contact and ensure communication.
The author responsible for distribution of materials integral to the findings presented in this article in accordance with the policy described in the Instructions for Authors (https://academic.oup.com/plphys/pages/general-instructions) is: Xuhui Zhou, (xhzhou@des.ecnu.edu.cn).

Abstract

Increasing sea levels associated with climate change threaten the survival of coastal forests, yet the mechanisms by which seawater exposure causes tree death remain poorly understood. Despite the potentially crucial role of nonstructural carbohydrate (NSC) reserves in tree survival, their dynamics in the process of death under seawater exposure are unknown. Here we monitored progressive tree mortality and associated NSC storage in Sitka-spruce (*Picea sitchensis*) trees dying under ecosystem-scale increases in seawater exposure in western Washington, USA. All trees exposed to seawater, because of monthly tidal intrusion, experienced declining crown foliage during the sampling period, and individuals with a lower percentage of live foliated crown (PLFC) died faster. Tree PLFC was strongly correlated with subsurface salinity and needle ion contents. Total NSC concentrations in trees declined remarkably with crown decline, and reached extremely low levels at tree death (2.4% and 1.6% in leaves and branches, respectively, and 0.4% in stems and roots). Starch in all tissues was almost completely consumed, while sugars remained at a homeostatic level in foliage. The decreasing NSC with closer proximity to death and near zero starch at death are evidences that carbon starvation occurred during Sitka-spruce mortality during seawater exposure. Our results highlight the importance of carbon storage as an indicator of tree mortality risks under seawater exposure.

Received July 13, 2020. Accepted December 9, 2020. Advance access publication January 25, 2021

Introduction

Sea level rise is anticipated to increase in frequency and magnitude as a result of climate change, widely impacting coastal terrestrial ecosystems in upcoming decades (Kemp et al., 2011; IPCC, 2014; Buchanan et al., 2017). Coastal forests, located at the interfaces of sea and land, are considered as one of the most vulnerable ecosystems to climate change (Desantis et al., 2007). Sea level rise increases the extent and duration of coastal inundation and seawater exposure, greatly threatening coastal forests in low elevations, leading to reduced tree growth, failure in regeneration, and forest mortality events (Williams et al., 1999; Fernandes et al., 2018; Ross et al., 2019; Wang et al., 2019). These vulnerabilities in coastal forests have caused profound impacts on coastal biogeochemical cycling by altering vegetation composition, water/carbon fluxes, and sediment transport (Kirwan and Megonigal, 2013; Krauss et al., 2018; Taillie et al., 2019). Although forest mortality events (e.g. "ghost forests") have been documented in many coastal regions (Kirwan and Gedan, 2019), little is known about the mechanisms of forest die-off under seawater exposure, hampering model predictions of future forest loss, and land conversion in response to sea level rise.

Nonstructural carbohydrates (NSCs), the primary metabolic energy reserve stored in plant tissues typically in the form of sugars and starch, play a critical role in growth and survival of plants under environmental stress (Chapin et al., 1990; Dietze et al., 2014). NSCs can function as buffer to metabolic demands when carbon supply is limited under environmental stresses such as drought, shade, and defoliation (Adams et al., 2013; Wiley et al., 2017; D'Andrea et al., 2019), and are crucial for tree resistance and resilience (Kozlowski, 1992; Hartmann and Trumbore, 2016). Higher NSC storage could increase tree survival rates under drought and insect outbreak (Quirk et al., 2013; O'Brien et al., 2014; Dickman et al. 2015; Trugman et al. 2018; Fierravanti et al., 2019). Under seawater intrusion scenarios, the main threats of salinity stress on plant physiology include the osmotic imbalance and toxic effects due to the excessive sodium (Na^+), chlorine (Cl^-), and the inhibition in uptake of other ions like calcium (Ca^{2+}), potassium (K^+), and nitrate (NO_3^-; Kozlowski, 1997). Both salinity stress and decreased freshwater availability can result in stomatal closure and CO_2 uptake reduction, which are accompanied by the growth decline in trees (Wang et al., 2019). Therefore, tree NSC storage depends in part on the asynchronies in the C supply and utilization. Insufficient NSC availability through reserve exhaustion or immobilization may cause tree death via interactions between the processes of carbon starvation and hydraulic failure or biotic agent attack (Sala et al., 2010; McDowell et al., 2011). Finally, tidal flooding damages roots via potential toxic compounds and increasing anaerobic decomposition due to decreased oxygen supply, limiting water, and nutrient uptake by roots (Kozlowski, 1997; Fagherazzi et al., 2019). In such stressful conditions, trees have to rely on their NSC storage for basic metabolism, osmotic adjustment, and phloem transport. However, to our knowledge, no study has been conducted to examine the NSC reserves during nonhalophyte tree death from seawater exposure.

Although many studies have focused on NSC responses to environmental stress (Dietze et al., 2014), how C starvation contributes to tree mortality is still debated as C depletion is not ubiquitously observed at mortality (Adams et al., 2017b). NSCs, especially low-molecular weight carbohydrates, should not decline to zero because of their multiple functions in maintaining metabolism and turgor (McDowell and Sevanto, 2010; Hoch, 2015). NSCs can also be maintained at a high level in some tissues due to transport failure, even in trees dying of the C starvation process (Sala et al., 2010; Wiley et al., 2017). However, an untested question is what minimum threshold levels of NSC (e.g. the concentrations) allow the tree to survive under seawater exposure. This lack of knowledge on NSC threshold prevents the mechanistic algorithm development of dynamic vegetation models and realistic prediction of tree responses to climate change (McDowell et al., 2011) including in coastline areas (Ward et al., 2020). One approach to quantify the NSC threshold is to monitor the NSC change throughout the process of tree death. However, most related studies have focused on NSC comparisons between surviving and dead trees, potentially missing key transition points at which trees start dying or cannot recover (Hammond et al., 2019; Sapes et al., 2019). In addition, most of the information is based on the observations on seedlings under highly controlled treatments like extreme drought or shade (Adams et al., 2017b; Wiley et al., 2017; Hartmann et al., 2018; Weber et al., 2018; but see Dickman et al., 2015).

Evidence is needed on NSC change throughout progressive mortality in mature forests caused by natural environmental stress, particularly in coastal forests under rapid, widespread but rarely studied disturbances. To address this challenge, we conducted a year-long study in a coastal forest undergoing rapid mortality from monthly tidal ecosystem-scale seawater exposure. The Sitka-spruce (*Picea sitchensis*) dominated floodplain located at Beaver Creek in the Pacific Northwest, USA provided an ideal cause-and-effect system for such a purpose (Figure 1A). Mature spruce trees previously growing under a freshwater-dominated environment were exposed to soil salinization after causeway removal in 2014, which allowed tidal seawater to move upstream and inundate adjacent floodplains at monthly frequency (Wang et al., 2019; Yabusaki et al., 2020). Overall, 78% of the Sitka-spruce trees died within 4 years of seawater exposure (Wang et al., 2019; Figure 1A). Sitka-spruce is an evergreen coniferous species that does not have the strategy of dropping leaves to reduce water loss like deciduous trees during stresses (Hasselquist et al., 2010). Nevertheless, Sitka-spruce has a rather isohydric performance that closes stomata and maintains constant xylem water potential, while reducing photosynthetic carbon gain during water stresses, which can increase the importance of carbon storage for survival (McDowell et al., 2008). The nonsprouter characteristics

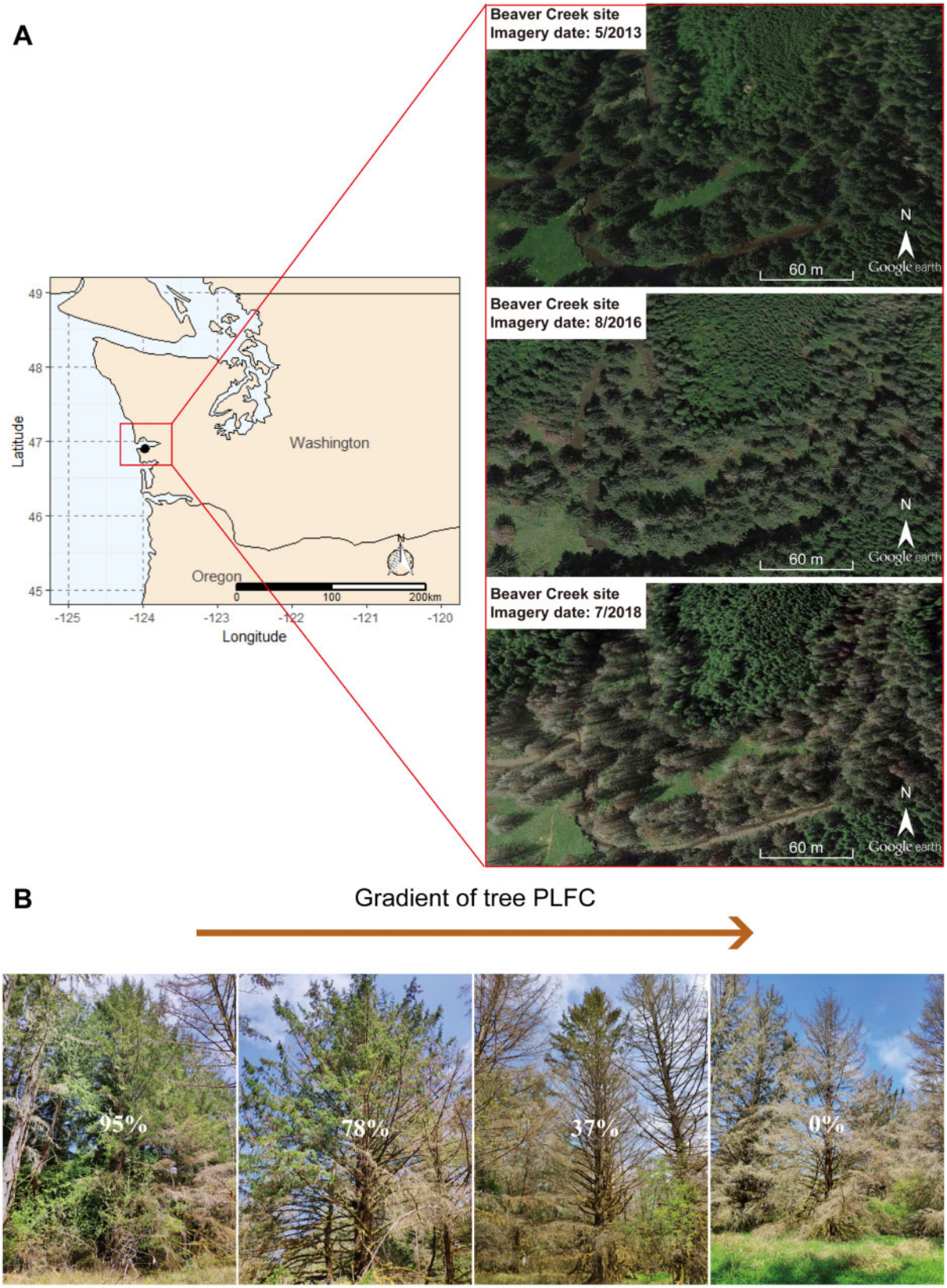

Figure 1 Site location and tree crown mortality estimation. A, The site is located at Beaver Creek, Washington, along the Pacific coast of the Pacific Northwest, USA. The spruce forest in this site was dying after causeway removal in 2014, shown in the satellite images from Google Earth. B, Examples of tree (%) estimation.

(Harris, 1990) also make trees more likely to fully utilize stored NSC rather than maintain reserves for resprouting events (Bond and Midgley, 2003). Finally, despite its coastal location, Sitka-spruce is a nonhalophyte and is thus sensitive to salinity. All these survival strategies may make the trees consume large amounts of stored NSC to cope up with the chronic saline stress caused by monthly seawater intrusion; thus, this species provides a good candidate for increasing our understanding of the role of carbon starvation in seawater intrusion-induced tree mortality.

Determining tree death is a challenging task, and there are various indicators across studies depending on discipline scales and research aims, including foliar color or defoliation, zero growth, cessation of maintenance respiration, or failure in recovery (McDowell et al., 2011; Hartmann et al., 2018; Hammond et al., 2019). Among them, the crown foliar change is the most intuitive and operational characteristic that is related to multiple physiological processes in nutrient metabolism, water transport, and carbon cycling, and has been used for large-scale monitoring to assess forest mortality risks (Gaylord et al., 2013; Poyatos et al., 2013; Neumann et al., 2017; Hartmann et al., 2018; Huang et al., 2019). Here we investigated crown health of trees (indicated by percentage of live foliated crown) regularly exposed to seawater by visual assessments (Figure 1B), simulated subsurface salinity, measured major ion contents in soil and needles, and determined NSC trends across a gradient of percentage of live foliated crown (PLFC). Our objectives were to (1) examine effects of salinity stress on tree decline, (2) identify patterns and responses of tree NSC storage to seawater intrusion-induced tree decline, and (3) determine the NSC threshold during the processes of tree death. We hypothesized that tree decline is highly related to salinity stress. Second, given the highly constrained carbon assimilation under seawater intrusion (Wang et al., 2019), we hypothesized that NSC and its component concentrations decline in concert with decreasing crown foliation.

Results

Percentage of live foliated crown and its relationship with soil and needle salinity

PLFC in Sitka-spruce trees, estimated by visual assessments on crown health, showed substantial decreases during sampling periods (Figure 2; Supplemental Table S1). Overall, the PLFC of these trees exposed to regular seawater intrusion decreased 66.7% from October 2018 to July 2019, and 7 of the 28 target trees died (i.e. PLFC reached to 0%; Figure 2A; Supplemental Table S2). The proportion of trees with low PLFC increased continuously during sampling periods (Figure 2B). At the end of sampling, 78.6% of target trees lost more than half of green foliage, 64.3% of target trees decreased PLFC below 25%, and 39.3% of target trees were with PLFC below 10% (Figure 2B). PLFC at each sampling time was highly related to the relative change from the last sampling time in May, June, and July ($P < 0.05$; Figure 3). Trees with less PLFC showed a greater relative reduction of live foliated crown by the next sampling (Figure 3). Particularly, trees with PLFC below 25% showed sharper decreases of live foliated crown than those with PLFC above 25% in May, June, and July (Figure 3). In addition, trees with lower PLFC had accelerated crown decline over time, while trees with higher PLFC did not (Supplemental Figure S1). No correlation was found between tree diameter and PLFC ($P > 0.05$).

To assess salinity stress on each tree, we examined soil and needle ion contents, and simulated subsurface salinity at each target tree location. Tree PLFC and its rate of decrease were highly related to the simulated subsurface salinity ($P < 0.001$; Figure 4, A and E). Meanwhile, PLFC decreased significantly with increasing needle Na^+ and Ca^{2+} contents and decreasing needle K^+ contents ($P < 0.05$; Figure 4, B–D), but not significantly with needle Mg^{2+} and soil ion contents ($P > 0.05$; Figure 4, B–D; Supplemental Figure S2A). The rates of PLFC decrease in the dry season (March–July) were positively related to Na^+ and Ca^{2+} contents in needles, except needle K^+ and Mg^{2+} (Figure 4, F–H; Supplemental Figure S2B). Needle K^+ contents were negatively correlated with the decreased rates of PLFC ($P < 0.05$; Figure 4G), and needle Mg^{2+} contents were not correlated with the decreased rates of PLFC ($P > 0.05$; Supplemental Figure S2B).

Shoot water potential

Shoot water potential at predawn and mid-day showed no significant change with sampling time or PLFC ($P > 0.05$; Figure 5, Supplemental Table S3). Predawn water potential became significantly more negative with increasing needle Ca^{2+} contents and decreasing needle K^+ contents (correlation coefficients are −0.31 and 0.36, respectively, $P < 0.05$; Figure 6), and became marginally more negative with increasing needle Na^+ contents and simulated subsurface salinity ($P = 0.05$ and 0.08, respectively; Figure 6, Supplemental Figure S3). No significant correlations were observed between predawn water potential and tissue NSC concentrations ($P > 0.05$; Figure 6).

Carbohydrates in relation to PLFC

Concentrations of NSC and its components varied with tissue, time, and PLFC ($P < 0.05$; Supplemental Table S4). In October, the concentrations of NSC and its components were the lowest (Supplemental Figure S4), and there was a lack of relationship between PLFC and NSC concentrations (and its components) except in root starch and branch sugars (Figure 7). In March and May, NSCs in all tissues were found to decrease significantly with declining PLFC ($P < 0.001$; Supplemental Table S5). In June and July, significant correlations between NSC concentrations and PLFC were observed in stems and roots (Figure 7A; Supplemental Table S5). The change of starch with PLFC was consistent with the correlations between total NSC and PLFC (Figure 7B; Supplemental Table S5). Soluble sugar concentrations in branches, stems, and roots were positively related to

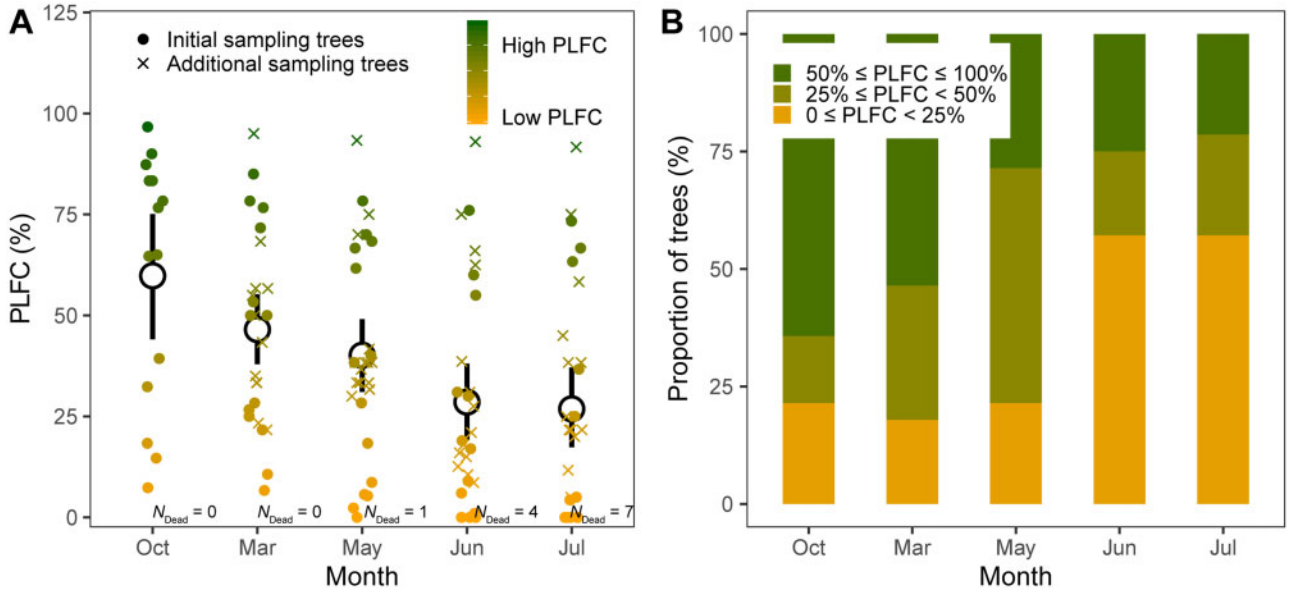

Figure 2 The dynamics of tree death over time. A, The dynamics of tree PLFC during sampling periods. Data points are staggered to reveal overlapping points. Different colors of points refer to the gradient of PLFC. Central circles and bars indicate mean values with 95% confidence interval. Solid circles refer to PLFC of the initial 14 target trees; crosses refer to PLFC of the 14 more target trees added to increase sampling sizes from March 2019. Numbers near points refer to the amounts of dead trees (i.e. PLFC = 0%) within the 14 or 28 sampling sizes. *Lmer* analysis showed that PLFC changed significantly with time (*F*-value = 31.64, $P < 0.001$; Supplemental Table S1). B, The proportion of trees with 50% ⩽PLFC ⩽ 100%, 25% ⩽ PLFC < 50%, and PLFC < 25% over sampling periods.

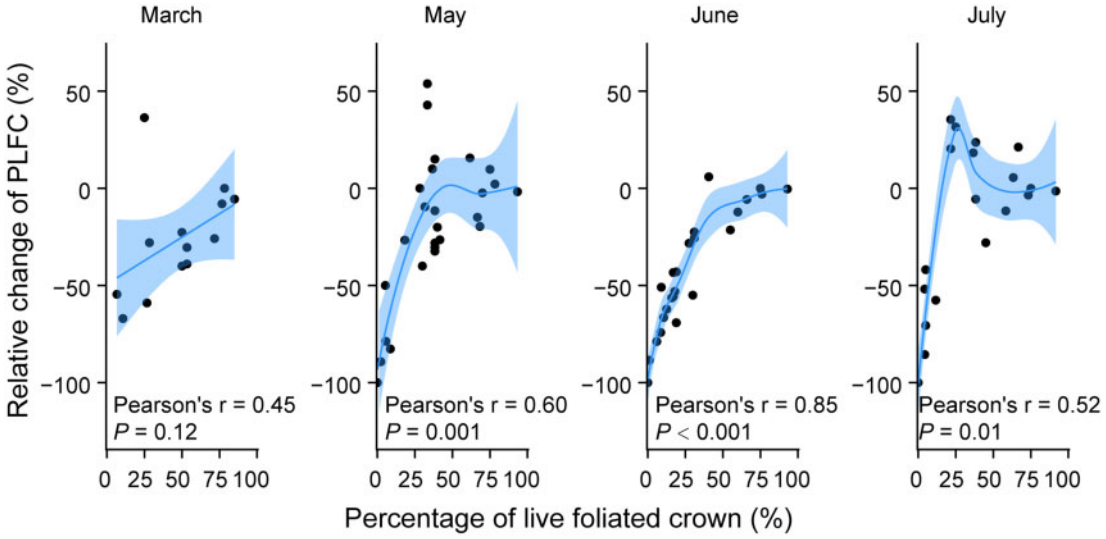

Figure 3 Relationships between the PLFC at each sampling time and relative change of PLFC compared to last sampling time. Either a linear or loess function (blue line) was chosen to better represent the relationships. Shaded areas represent 95% confidence intervals for predictions. Note that the occasional appearance of positive values of relative change of PLFC is due to the error in the estimation of PLFC. The comparisons of PLFC among sampling time for each tree are shown in Supplemental Table S2.

PLFC, but their relationships were variable with time and tissue types (Figure 7C; Supplemental Table S5).

Across the entire sampling period, concentrations of total NSC, sugars, and starch in tree tissues all decreased nonlinearly as PLFC reduced, with the exception of leaf sugars (Figure 7 and Table 1). NSC concentrations decreased more in stems and roots (88.0% and 85.1%, respectively) than those in leaf and branches (64.9% and 66.0%, respectively) from 100% to 0% PLFC (Figure 7 and Table 1). Similarly, sugar concentrations in stems and roots decreased much more than those in leaves and branches from 100% to 0% PLFC (Figure 7 and Table 1).

Starch showed remarkably large decreases in all tissues (94.0%, 73.2%, 81.6%, and 89.0% in leaves, branches, stems, and roots, respectively) as PLFC decreased (Figure 7 and Table 1). Meanwhile, when complete crown death occurred

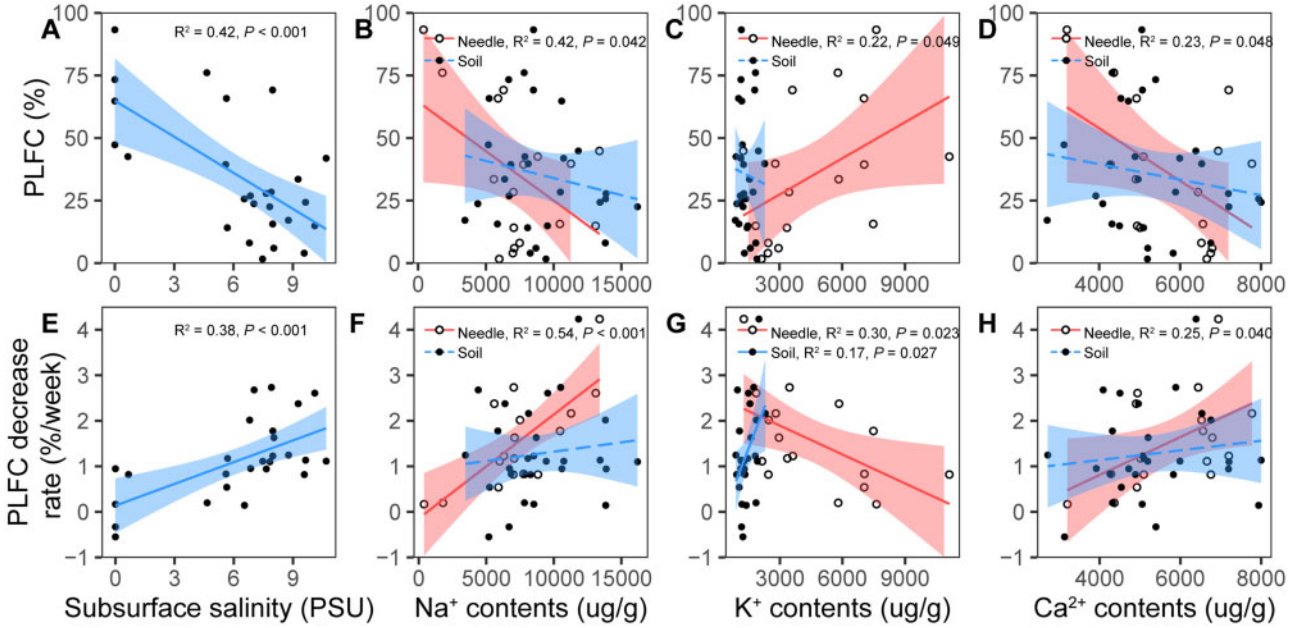

Figure 4 Relationships of crown mortality with needle/soil salinity. A–D, Relationships of PLFC with modeled subsurface salinity, and with needle and soil Na^+, K^+, and Ca^{2+} contents. E–H, Relationships of PLFC decreasing rates with subsurface salinity, needle/soil Na^+, K^+, and Ca^{2+} contents. PLFC, needle/soil Na^+, K^+, and Ca^{2+} contents for each tree were the average value from March 2019 to July 2019. Subsurface salinity was averaged from simulated values at the 5, 15, 25, 35, and 45 cm depth from March 2019 to July 2019. Decrease in rates of PLFC were calculated by the decrease in slope of PLFC during the sampling period. Shaded areas represent 95% confidence intervals for predictions from a linear model. Dashed lines indicate insignificant linear regressions ($P > 0.05$).

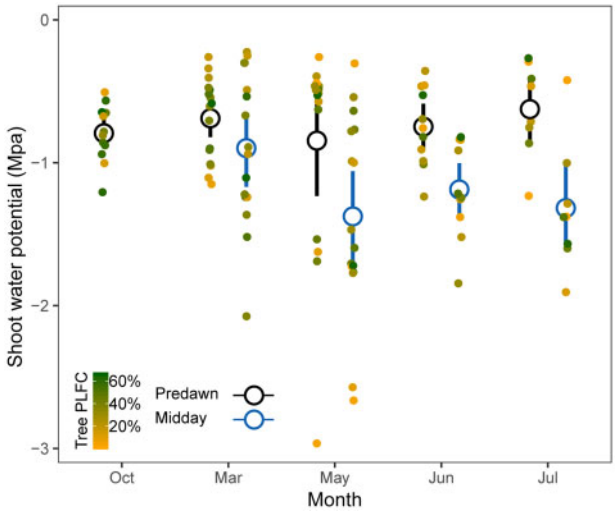

Figure 5 Shoot water potential dynamics over time. Data points are staggered to reveal overlapping points. Different colors of points refer to the PLFC. Black and blue central circles with bars indicate mean predawn and mid-day water potential with 95% confidence interval, respectively. *Lmer* analysis showed that predawn and mid-day water potential did not change with time (*F*-value = 0.30, $P = 0.88$ for predawn water potential; *F*-value = 0.24, $P = 0.87$ for mid-day water potential; Supplemental Table S3).

(at 0% PLFC), concentrations of NSC and its components in stems and roots decreased to as low as <0.5% (Figure 7 and Table 1). At crown death, leaf/branch starch reached as

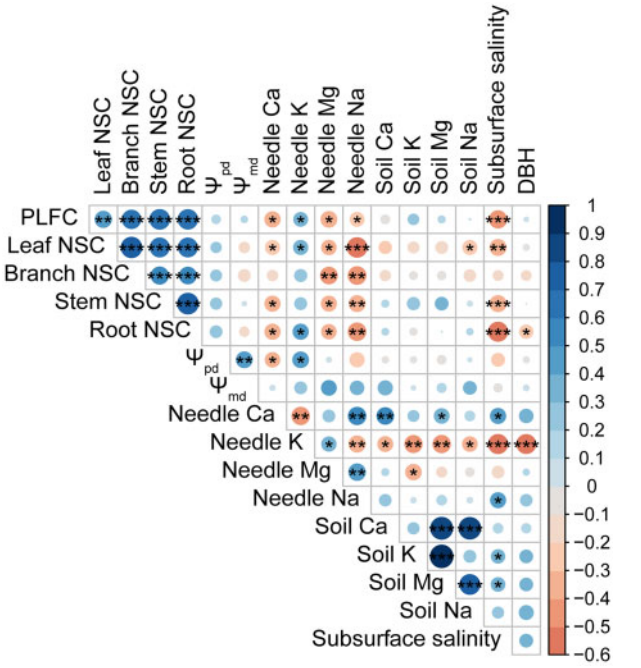

Figure 6 Correlation matrix for PLFC, tissue NSC concentrations, shoot predawn and mid-day water potentials (Ψ_{pd} and Ψ_{md}), ions (Na^+, K^+, Ca^{2+}, Mg^{2+}) contents in needles and soil, modeled subsurface salinities, and stem diameters at breast height (DBH). The color of each circle represents the correlation coefficient (scale to right of matrix). The size of the circle and asterisks represent the significance level (*$P < 0.05$; **$P < 0.01$; ***$P < 0.001$).

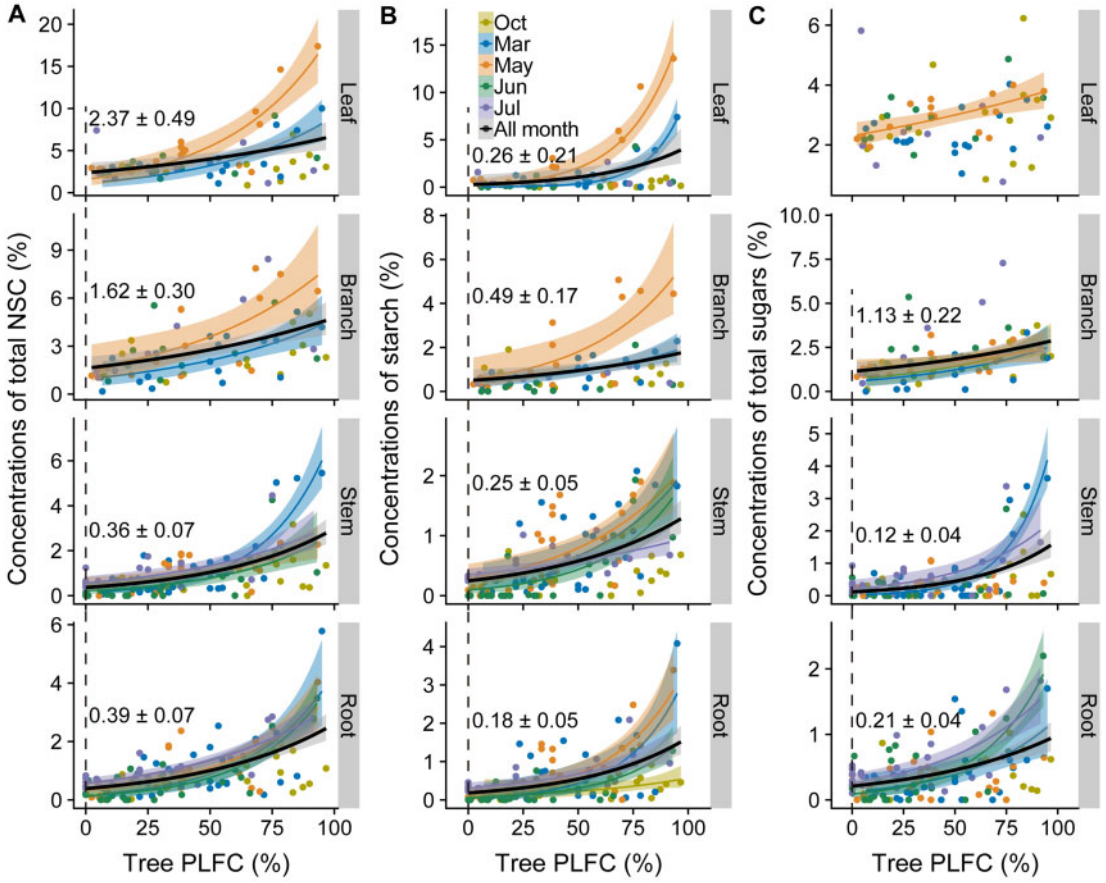

Figure 7 Relationships of crown mortality and carbohydrates. Relationships between PLFC and total NSC (A), starch (B), and soluble sugars (C) concentrations in leaves, branches, stems, and roots. Colors within each panel represent the sampling months: October (tawny), March (blue), May (orange), June (green), and July (purple), all months combined (black). The fitted model is GLMs with log links. Shaded areas represent 95% confidence intervals of the regression lines. Only significant regressions are shown ($P < 0.05$, details of model predictions are in Table 1 and Supplemental Table S5). Values shown in each panel are the concentrations of NSC (or its components, ± SE) predicted at 0% PLFC from significant regressions overall the sampling periods.

low as stem/root starch, but total NSC and total sugar concentrations in leaves/branches were still higher than those in stems/roots (Table 1). No significant correlations were found between time to crown death and tissue sugar concentrations ($P > 0.05$). However, starch concentrations decreased as the crown approached death. The time to crown death correlated positively with starch storage in woody tissues (branches, stems, roots) but not in leaves from March to July of 2019 (Figure 8).

Discussion

Tree death after exposure to seawater

Trees at the Beaver Creek floodplain experienced declining PLFC caused by regular tidally driven seawater intrusion. The rates of decline were highly related to soil salinity exposure controlled by topography (Figures 2 and 4). This crown dieback and ultimate death is in line with previously observed drastic reductions in tree growth after onset of seawater intrusion in 2014 at this site (Wang et al., 2019). Both tree growth decline (Camarero et al., 2015; Cailleret et al., 2019) and reducing crown condition (Gaylord et al., 2013; Poyatos et al., 2013) in trees are considered to be early warning signals of tree mortality risks. In this system, the crown decline was faster for trees with lower initial percentage of live foliage (Figure 3). The correlation between crown decline rate and salinity stress levels (Figure 4) suggests that tree survival time largely relies on the individual physiological resistance to salt uptake and heterogeneous salinity stress in field settings.

The acceleration of crown foliage loss with worse crown status (Figure 3) indicates that trees become increasingly vulnerable as PLFC declines. This response pattern is expected based on the combined effect of saline stress and its cumulative negative impacts on tree physiology. The rainfall contribution to salinity dilution is limited due to the low permeability and the ponding of saline creek water on the floodplain; thus, persistent salt accumulation occurred with frequent seawater intrusion (Yabusaki et al., 2020). The higher needle salinities in faster dying trees should cause increasing osmotic stress and ionic toxic damage on trees. More energy or resources are needed for maintaining

Table 1 Model predictions for NSC and its component concentrations as function of PLFC over all the sampling periods

NSC and its components	Tissue	Intercept	*P*-value	Slope	*P*-value	Df (res.)	Value at 100% PLFC (±SE)	Value at 0% PLFC (±SE)	NSC decrease%
Total NSC	Leaf	0.86	**<0.001**	0.01	**<0.001**	64	6.75 ± 0.91	2.37 ± 0.49	64.89
	Branch	0.48	**0.011**	0.01	**<0.001**	64	4.77 ± 0.57	1.62 ± 0.30	66.04
	Stem	−1.02	**<0.001**	0.02	**<0.001**	124	2.99 ± 0.32	0.36 ± 0.07	87.96
	Root	−0.95	**<0.001**	0.02	**<0.001**	124	2.61 ± 0.26	0.39 ± 0.07	85.06
Starch	Leaf	−1.36	0.098	0.02	**0.006**	64	4.31 ± 1.10	0.26 ± 0.21	93.97
	Branch	−0.71	**0.049**	0.01	**0.010**	64	1.83 ± 0.37	0.49 ± 0.17	73.22
	Stem	−1.40	**<0.001**	0.02	**<0.001**	124	1.36 ± 0.16	0.25 ± 0.05	81.62
	Root	−1.70	**<0.001**	0.02	**<0.001**	124	1.63 ± 0.22	0.18 ± 0.05	88.96
Total sugars	Leaf	0.88	**<0.001**	0.003	0.112	64	3.10 ± 0.28	2.41 ± 0.22	22.26
	Branch	0.12	0.517	0.01	**0.001**	64	2.95 ± 0.39	1.13 ± 0.22	27.80
	Stem	−2.15	**<0.001**	0.03	**<0.001**	124	1.71 ± 0.27	0.12 ± 0.04	92.99
	Root	1.56	**<0.001**	0.02	**<0.001**	124	0.99 ± 0.12	0.21 ± 0.04	78.79

GLMs with log links were selected to best fit by AIC. The predicted values of NSC (and its components) concentrations at health (100% PLFC) and death (0% PLFC) were included. Percentage of NSC decrease from health to death was calculated by the predictions. The *P*-value is shown in bold at the 0.05 significance level. Model predictions for each sampling time are in Table S5

metabolism and growth (e.g. more carbohydrates are required as the solutes for osmotic balance; Kozlowski, 1997; Tattini et al., 2002). In addition, leaf shedding is an inevitable consequence of water stress (Poyatos et al., 2013). Reduced leaf area decreases carbon fixation, forcing trees to use stored C for metabolic activities (D'Andrea et al., 2019). Continual depletion of NSC storage could thus enhance tree vulnerabilities to stress (Aguade et al., 2015). Moreover, we found that the tree health decline accelerated during the drier summer, especially for those with PLFC below 25% (Figure 3). We speculated that this result is likely due to the compounding effect of increased soil salinity, reduced precipitation, and warmer temperatures in summer. Increased temperature has been found to exacerbate the extent and rate of tree mortality in other natural and experimental studies (Breshears et al., 2005; Adams et al., 2009, 2017a; Duan et al., 2018). This acceleration is assumed to be related to enhanced water and, potentially, carbon limitations under increased air temperature (McDowell et al., 2018). In such cases, large loss of leaves may make trees more sensitive to multiple environmental stresses. These combined negative effects have great implications on vulnerabilities of coastal forests and subsequent biogeochemical cycles in coastal ecosystems, as sea level extremes, precipitation reductions, and heat waves are expected to increase in future years (IPCC, 2014).

NSC declines during tree death

We observed a significant NSC decline during tree death in response to seawater exposure. The negative carbon balance in trees was not only clearly shown by the NSC patterns among trees with different PLFCs (Figure 7), but also accurately predicted the time to death (Figure 8). The depletion of starch to approximately zero at death, along with very low growth prior to death (Wang et al., 2019), are consistent with carbon starvation in trees (defined both as a process of depletion and an endpoint of zero starch; McDowell et al., 2011). The carbon starvation due to depleted carbohydrates and hydraulic failure by xylem dehydration are two main hypotheses for the physiological cause of tree mortality (Adams et al., 2017b). Although hydraulic failure appears to be ubiquitous during drought, it is common but not universal for a tree to die with carbon depletion under stress (Maguire and Kobe, 2015; Piper and Fajardo, 2016; Wiley et al., 2016, 2017; Adams et al., 2017b). In this study, predawn shoot water potential became more negative with the increase of needle Na^+, Ca^{2+} contents, and subsurface salinity (Figure 6; Supplemental Figure S3), suggesting an increase in salinity stress that impeded hydraulic function in trees. Significant relationships between PLFC and NSC reserves in trees indicate gradual carbon depletion in these seawater-exposed trees. The occurrence of carbon starvation in our study does not preclude the process of hydraulic failure from co-occurring, as the loss of NSCs can promote embolism (Sevanto et al., 2014). Here we did not try to distinguish which of the two mechanisms caused tree death, but aimed to improve understanding of how NSC dynamics respond to mortality induced by seawater exposure. The large use of NSC in Sitka-spruce trees exposed to seawater might be largely attributed to their isohydric, nonsprouting, and non-halophytic behavior under stress. This NSC depletion and carbon starvation occurring in trees under salinity stress needs to be examined in more detail with other coastal tree species and ecosystems.

Our investigation on Sitka-spruce trees with a gradient of tree health status provides a continuous temporal NSC pattern in the process of death with variable environmental factors. The seasonal NSC dynamics were consistent with the previous observations in temperate species that NSC decreased in dormant seasons and increased in the growing seasons (Martínez-Vilalta et al., 2016; Furze et al., 2019). Meanwhile, in October, the lack of relationship between NSC and tree crown health except in root starch and branch sugars (Figure 7), indicates that NSC in healthy trees decreased to levels comparable with declining trees. This may result from the consumption of starch at the end of growing seasons. Combined with the higher soil salinity levels in October (Supplemental Figure S5B), the lower NSC levels may increase risks of tree mortality at this time (O'Brien et al., 2014). However, our results showed that the

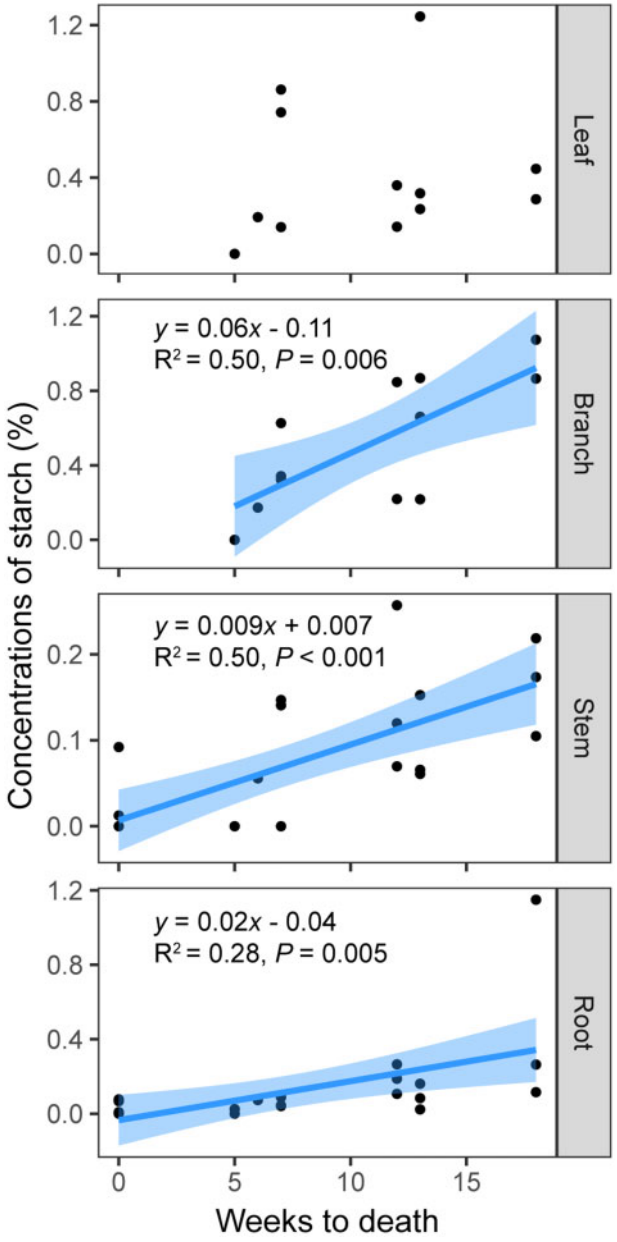

Figure 8 Starch storage in woody tissues (branches, stems, roots) in response to trees' weeks to complete death. Trees' weeks to complete death were estimated based on the time when 0% PLFC in each crown was found (the week of 0% PLFC was week zero). Each prior sampling period was then used to populate the regression. Only significant regressions are shown ($P < 0.05$). Shaded areas represent 95% confidence intervals of the regression lines.

seasonal tree decline rates were largely regulated by tree crown health status (Supplemental Figure S1), suggesting the limited role of seasonal NSC fluctuations in tree mortality.

We found that total NSC concentrations can decrease to 2.4% and 1.6% in live leaves and branches, and to ~0.4% in live stems and roots, indicating the starved status in seawater-exposed trees at death. Particularly, starch in all tissues was almost completely consumed at death (Figure 7 and Table 1). Our records are much lower than the minimum NSC observed at death in some prior studies (e.g. dead leaves of shade-treated aspen: 4%–7.5%; live root segments from decaying coarse roots: ~5%–6%; dead leaves of pine during drought: 4%; and roots of dead trees after beetle attack: ~2%; (Adams et al., 2013; Wiley et al., 2016, 2017), but similar to the NSC observation on dying seedlings and saplings in shade studies (Sevanto et al., 2014; Weber et al., 2018; Wiley et al., 2019), and CO_2-starvation studies (Hartmann et al., 2013a; Quirk et al., 2013). The consistency of our low starch/NSC values at death with those of extreme shade and CO_2-starvation studies suggests that our trees did experience carbon starvation, as it is defined (Sala et al., 2010; McDowell et al., 2011). However, we noted that other causes of variation in starch depletion minima during stress could result from historically different carbohydrate analysis methods (Quentin et al., 2015; Landhäusser et al., 2018), and species and environmental differences (Wiley et al., 2019). Despite that, most of the studies were conducted on seedlings or small trees. Our observations provide evidence of extreme NSC depletion in large trees under field conditions when trees die of seawater exposure.

Our NSC measurements on dying trees based on foliar presence assessment may underestimate the lethal NSC threshold, otherwise known as a point-of-no-return (Hammond et al., 2019; Sapes et al., 2019). Death symptoms occur asynchronously in morphology (e.g. foliar browning or defoliation) and physiological function (e.g. cessation of respiration, failure in water transport, or their irreversible points; Hartmann et al., 2018). It is thus possible that trees have passed the point of no return when the crown die-back is observed (Hammond et al., 2019). However, some trees can still survive at extreme levels of hydraulic failure after drought relief (Hammond et al., 2019). These data suggest that the point of no return can be variable, involving multiple interacting physiological traits and processes. Moreover, crown status under stress has been often regarded as a comprehensive indicator of tree vigor linked to levels of the key physiological function (Galiano et al., 2011; Poyatos et al., 2013), and crown die-back should be somewhere between the point of severe stress and the point of cessation of tissue respiration (Garcia-Forner et al., 2016). Through tracking the stored carbohydrates with the variable crown die-back levels, we were able to detect the C balance dynamics in the processes of dying and its role in determining tree survival time.

The NSC minima were similar among sampling times but varied with tissues. When trees fully died, leaves stored more NSC (especially sugars) than the other tissues, which was consistent with the sugar distributions in trees at death induced by drought, shade, or insect attack in other studies (Hartmann et al., 2013b; Wiley et al., 2016, 2017). The higher sugar requirements for osmotic maintenance in leaves or the phloem transport failure are assumed to cause this pattern of higher sugar content in above- than below-ground tissues (Wiley et al., 2019), thus leading to relatively higher

sugar concentration in leaves at death (McDowell and Sevanto, 2010). The sugar maintenance in leaves may be contributed by the remobilization of existing pools, like transforming starch to soluble forms or translocating sugar for demands (Hartmann et al., 2015). Foliar salinity stress should exacerbate these drivers, because low-molecular weight sugars are needed for osmoregulation (Greenway and Munns, 1980). However, very low levels of sugars in stems and coarse roots at tree death indicate the gradual depletion of carbohydrates in these tissues. Indeed, trees can still survive with near-zero sugar storage, which was probably attributed to the use of alternative C sources like lipids, proteins, or hemicelluloses (Weber et al., 2018).

In contrast with sugars, starch was exhausted in all tissues by the point of death. This result is consistent with other studies on NSC responses under stresses both in mature trees and seedlings, where almost all starch was consumed, particularly in woody tissues (Klein et al., 2014; Mitchell et al., 2014; Wiley et al., 2016, 2017; Weber et al., 2018), although it is possible that a portion of starch is inaccessible for mobilization or hydrolysis (Millard et al., 2007). In leaves, the sugar maintenance combined with the exhaustion of starch suggests a full consumption of starch to sugars for survival. Our results also showed that the time to tree death was strongly related to starch storage in woody tissues (Figure 8), which has been shown previously for drought studies (O'Brien et al., 2014; Dickman et al., 2015). Hence, starch reserves in trees may be a reliable indicator of starvation during regular seawater exposure, and a potential predictor of tree survival time under stresses.

Conclusions

Our study found that crown foliage and tissue NSC concentrations of Sitka-spruce trees simultaneously declined under regular tidal seawater exposure. These results, combined with declining growth, suggest that carbon starvation was a driver of tree mortality induced by seawater intrusion. The death process was associated with the depletion of NSC stores. At death, starch in the trees was almost completely consumed, but sugars were maintained at higher levels in foliage than in stems and roots. This suggests that starch depletion—particularly in woody tissues—is a more reliable indicator of carbon starvation in trees. Considering the expected increase in sea level, and the frequency and magnitude of storm surge, drought, and heat-waves events, further studies are needed on the variation in NSC thresholds to better assess tree mortality risks and coastal forest vulnerability under climate change.

Materials and methods

Site information

Our study was conducted in an evergreen Sitka-spruce (*Picea sitchensis*) forest that was over 100 years old, located along Beaver Creek (46° 54′ 25.2″ N, 123° 58′ 33.6″ W) on the Washington coast of the Pacific Northwest, USA (Figure 1A). The climate is characterized by cold, humid winters and warm, dry summers. Historic (1950–2017) mean annual air temperature is 10.2°C and mean annual precipitation is 1,919.4 mm, with most rainfall occurring in the October–March wet seasons (Supplemental Figure S5A). Beaver Creek is a first-order tributary of the Johns River that drains into the Grays Harbor estuary, approximately 1.5 km from the area. The stream was previously dominated by freshwater, with tidal access prevented by a causeway near the river mouth (Sengupta et al., 2019). Tidal access was restored in 2014 by removal of the causeway for fish passage and rearing habitat (Washington Department of Fish and Wildlife, 2019). Since then, Beaver creek has experienced a daily tidal range of ∼2 m and extreme flooding events that inundate the floodplain at quasi-monthly frequency (Yabusaki et al., 2020). The monthly durations of floodplain inundation range from 9.5 h (summer) to 44 h (winter), with monthly peak water levels fluctuating from 2.8 m (summer) to 3.3 m (winter). The floodplain has been at the early stage of salinization through exposure to frequent tidal water levels, with current ground water salinity ranging from 6.1 practical salinity unit (PSU) in May to 14.4 PSU in September (Yabusaki et al., 2020). Soil salinity in the floodplain varies seasonally with higher salinity occurring August to December (Supplemental Figure S5). The dominant trees on the floodplain (Sitka-spruce) have been dying rapidly since 2014 (Figure 1A). Our sampling was constrained to trees along a middle stretch of Beaver Creek located in the interface of a high salt-exposed area and a purely terrestrial upland, where the forest had >78% tree mortality (in 2018, Wang et al., 2019). The floodplain is a relatively flat area, and most of sampling trees distributed within the 2.5–2.8 m elevation interval of the floodplain. The elevations of stream bank and hillslope (∼3 m) are slightly higher than the central floodplain. During inundation events, tidal seawater entered the floodplain through low points along the stream bank.

Tree sampling and crown mortality

At the beginning of the study (October 2018), 14 live individuals were chosen as target trees along a gradient of PLFC from 7% to 97% (Supplemental Table S2). PLFC was estimated by averaging visual assessments from three persons from at least three positions around each tree, based on needle colors, leaf shedding, and branch desiccation (Figure 1B; Gaylord et al., 2013; Camarero et al., 2015). Sitka spruce is an evergreen species; thus, the original value of the full crown was estimated by the branched length of the crown, then the foliated fraction of that branched length was estimated. The foliage was presumed alive when green needles were present. A tree was considered dead when PLFC was 0% (i.e. crown was completely defoliated or has only brown needles; Adams et al., 2017b). From March 2019, 14 more sampling trees were added to increase the sample size, as we lost trees to complete crown death during the sampling period (Figure 2; Supplemental Table S2). All these target trees were distributed close to each other on the floodplain of the midstream (within an area of

120 m × 60 m), and their stem diameters at breast height ranged from 24.8 to 94.1 cm.

Leaf and core samples for NSC analyses were collected from the target trees on five sampling dates (October 2018, and March, May, June, and July 2019). On each sampling day, 1- and 2-year-old branches with green needles on the sun-exposed crown were sampled using a pole pruner. Samples were always collected around noon and were immediately kept in a 0–4°C cooler with ice after separation from trees (Landhäusser et al., 2018). The outer 3-cm stemwood cores with dead bark removed were taken with a 5.15-mm increment borer at about 1.3 m above the ground on the southern hemisphere of the tree. The outer 3-cm cores of coarse roots were collected from the main roots (with diameters of ∼10 cm) located close to the trunk at the soil depth of 5–10 cm using the increment borer.

Subsurface salinity and major ions in soil/needles

We assessed salinity stress on each target tree using soil and needle ion analyses and through calibrated model estimates of soil salinity. The simulated salinities represent time-resolved porewater salinity in the vadose zone, whereas the discrete soil samples represent a snapshot of soil ionic content at the time of sampling.

We sampled needles and under-tree soil for major ions (sodium, potassium, calcium, magnesium; Na^+, K^+, Ca^{2+}, Mg^{2+}) analyses from the same 14 or 28 target individuals as PLFC estimation. This sampling was carried out during field campaigns in October 2018, and March and May 2019. Three soil samples were collected through excavating from three directions and within a distance of ∼50 cm from the stem base of each tree to a depth of 5–10 cm. For each tree, the three soil samples were pooled for further analyses. Needles were separated from the collected branches. After air drying and grinding into powders, soil or needle samples were acid-digested, and the concentrations of the major ions in samples were analyzed via ion coupled plasma-optical emission spectrometry (ICP-OES). Following digestion by trace metal-free (TMF) concentrated nitric acid, TMF concentrated hydrochloric acid, TMF hydrogen peroxide, and resuspension in deionized water, the final sample was weighed and subtracted from the tare weight to calculate the mass of the digestates and ultimately the density of the digestate. The digestates were analyzed directly on a Perkin Elmer 7300 DV system ICP-OES for Ca, Mg, K, and Na. A two-point calibration was used, a blank and a high standard. The calibration was verified using a second source standard for all analyzed analytes. Continuing calibration verification standards and blanks were run every 10 samples. An internal standard was added online and was used to correct for any matrix effect from the samples. Method blanks were below detection limits. Data are reported as μg/g dry weight.

We also simulated salinization of the floodplain (Yabusaki et al., 2020) and identified subsurface porewater salinity at each target tree location. A three-dimensional variably saturated flow and salinity transport model of the floodplain (Yabusaki et al., 2020) was developed using the PFLOTRAN Richards Equation simulator (Hammond et al., 2014). In brief, the PFLOTRAN model used 1-year of 30-min frequency observations (continuously monitored from April 2018 to April 2019) of water level and salinity from the stream and hillslope groundwater well as input. Salinity in wells was converted by field monitored electrical conductivity and pressure readings. The model domain had 61 discrete elevations of ground surface (based on the 2009 DEM; LiDAR Bare Earth DEM, 2010), ranging from 1.2 to 7.2 m. By repeated applications of the 1-year dataset of boundary conditions, salinization of the floodplain from restoration of tidal access in 2014 to the end of our study period (July 2019) was constructed. Since our sampling trees were distributed on the same floodplain where the subsurface salinity was modeled, we were able to simulate tree-specific porewater salinity during the study period according to the spatial information of trees. Depth-resolved (5-, 15-, 25-, 35-, and 45-cm depth) time histories of porewater salinity at each tree location were part of the model output generated at an hourly frequency with 3-m lateral and 0.1-m vertical resolution. For each depth below a tree location, results were output 24 times each year, which corresponded to monthly maximum water level at the experimental floodplain and the immediately subsequent local minimum (average 7.5 h later). The model results were validated against our continuous time series data from our primary wells as well as with measured water levels and salinity from the nearby creek and two additional floodplain wells (Yabusaki et al., 2020).

Shoot water potential

On the sampling days of March, May, June, and July 2019, shoot water potential for each target tree was measured on two terminal shoots at predawn (∼3:00–5:00) and mid-day (∼11:30–13:30) using a Scholander-type pressure chamber (PMS Instruments, Corvallis, OR, USA), and determined by the average of two samples. Shoot water potentials were only measured at predawn in October 2018, as no mid-day samples were collected because of heavy cloud cover.

Nonstructural carbohydrates

Samples for carbohydrate analysis were microwaved at 700 W for 90 s within 5 h after collection (well within the acceptable time limit of 48 h; Landhäusser et al., 2018). After returning to the lab, samples were dried in an oven at 65°C for 72 h and then ground into powders of <0.15 mm particle size with a ball mill (SPEX SamplePrep 2010 Geno/Grinder, Metuchen, NJ, USA). NSC extraction and quantification of samples were carried out following the protocols in Landhäusser et al. (2018). Two inter-lab standards (peach leaves NIST1547 and pinon needles; Dickman et al., 2019) and one synthetic standard (Landhäusser et al., 2018) were also applied in the analyses. Briefly, each ground sample was extracted in 80% (v/v) ethanol at 90°C. The supernatant obtained after centrifuging was used for soluble sugar (i.e. glucose, fructose, and sucrose) quantification. To determine the sugar concentrations, sucrose was broken down to

glucose and fructose by invertase (Sigma cat. no. I9274), while glucose and fructose were phosphorylated to glucose-6-phosphate by hexokinase (Sigma cat. no. G3293) with isomerase (Sigma cat. no. P5381-5KU). Glucose-6-phosphate concentration was determined photometrically in a 96-well microplate reader (ELx800UV, BioTek Instruments, Winooski, USA) by measuring the increase in absorbance at 340 nm as NAD + was reduced to NADH. The ethanol-insoluble residual separated after extraction was used for starch digestion after ethanol evaporation. Starch in the pellet was hydrolyzed to water soluble glucans using α-amylase from *Bacillus licheniformis* (Sigma cat. no. A4551). After removal of structural carbohydrates by centrifuge, the glucans contained in the supernatant were hydrolyzed into glucose by amyloglucosidase from *Aspergillus niger* (Sigma cat. no. ROAMYGLL). The glucose hydrolysate was quantified as the glucose quantification above. Starch concentration was calculated by multiplying the glucose hydrolysate concentration by a conversion factor of 0.9. The total NSC was calculated as the sum of starch and soluble sugar concentrations as percentage of dry matter (% dry matter).

Notably, the original dilution factor (5×) of sugar extracts shown in the protocols of Landhäusser et al. (2018) was found not suitable for low sugar (<0.5%) measurements on some samples collected from dying trees in our site. Through a preliminary test and validation, we found that by changing the dilution factor to 10× it was able to detect the sugar signals with concentrations <0.5% (details described in the Supplemental Method S1). Therefore, 10× dilution was used in the sugar analyses on all samples.

Statistics

We tested the change of PLFC and shoot water potential within sampling periods using repeated measures of linear mixed-effects (LMEs) models fit by maximum likelihood through *lmer* function of lme4 package in the program R, and calculated *P*-values based on Satterthwaite's approximations. Each individual tree was considered as a repeated measure factor. Tree PLFC was used as covariates in analyzing the change of shoot water potential. Fixed effects of tissues, sampling time, and their interactions on concentrations of total NSC, sugars, and starch were also tested by the repeated measures of LME with PLFC as the covariates. Data were transformed by natural log or square root to achieve the normality of residuals. Pearson's correlations were done among PLFC, shoot water potentials, concentrations of NSC and its components, soil and needle major ion contents, and tree stem diameters.

The relative change of PLFC between sampling times was calculated by [(PLFC% − $PLFC\%_{last\ time}$)/$PLFC\%_{last\ time}$ × 100%] for each tree. Linear or loess functions were used to test the trends of relative change of PLFC with PLFC decreases, and their correlations were also tested by Pearson's correlation. PLFC for all target trees were found to decrease throughout the dry seasons (March–July), so we calculated the PLFC decrease rates during these months by the decrease in slopes fit by linear models. The correlations of PLFC and its decrease in rate with the simulated subsurface salinity and major ion contents in needles and soils were also evaluated by linear models.

We also performed generalized linear models (GLMs) with log links to predict the trends in NSC (and its components) concentrations with the PLFC change. The McFadden's pseudo-R^2 were used to assess the fits of these GLMs, and NSC (and its components) concentrations of tissues were predicted at the 0% and 100% PLFC. In addition, we estimated the weeks to complete death of trees based on the time when 0% PLFC was found at each investigation timepoint. Their correlations to tissue NSC (and its components) concentrations were evaluated by linear regressions. All statistical analyses were performed with the software R v. 3.5.1 (R Core Team, 2018).

Supplemental data

Supplemental Method S1. Measurement of sugars in samples with very low levels of sugars.

Supplemental Figure S1. Relative change rates of tree percentage of live foliated crown (PLFC) in each period $\frac{PLFC_{this\ sampling\ time} - PLFC_{last\ sampling\ time}}{Time\ interval \times PLFC_{last\ sampling\ time}}$.

Supplemental Figure S2. Relationships of crown mortality with needle/soil Mg^{2+} contents.

Supplemental Figure S3. Relationships of shoot predawn water potential (Ψ_{pd}) with soil/needle salinity.

Supplemental Figure S4. Carbohydrate dynamics in tree tissues.

Supplemental Figure S5. Climate and subsurface salinity in the site.

Supplemental Table S1. Results of the linear mixed models for the relationship between PLFC and month.

Supplemental Table S2. PLFC estimations at each sampling time (n = 3).

Supplemental Table S3. Results of the linear mixed models for the relationship between shoot water potentials (Ψ_{pd}, Ψ_{md}) and month.

Supplemental Table S4. Results of the linear mixed models for the effects of tissues, sampling time and their interactions on concentrations of total NSC, sugars and starch.

Supplemental Table S5. Model predictions for NSC and its component concentrations as function of PLFC at each sampling time.

Acknowledgments

We would like thank James Abend, Dekotah DeRoos, and Heather Pacheco for their assistance for field work and sample processing. This research is a part of the PREMIS Initiative at Pacific Northwest National Laboratory (PNNL). We thank Don Lentz, the Hancock Timber Company, and Washington Department of Fish & Wildlife for access to the Beaver Creek field site.

Funding

This research was funded by the Laboratory Directed Research and Development Program at Pacific Northwest

National Laboratory PNNL under Contract DE-AC05-76RL01830. X.Z. and P.Z. were supported by the National Natural Science Foundation of China (Grant nos. 31930072, 31770559, 31600387). P.Z. was partly supported by the East China Normal University scholarship for graduate students' short-term overseas research.

Conflict of interest statement. None declared.

References

Adams HD, Barron-Gafford GA, Minor RL, Gardea AA, Bentley LP, Law DJ, Breshears DD, McDowell NG, Huxman TE (2017a) Temperature response surfaces for mortality risk of tree species with future drought. Environ Res Lett **12**: 115014

Adams HD, Germino MJ, Breshears DD, Barron-Gafford GA, Guardiola-Claramonte M, Zou CB, Huxman TE (2013) Nonstructural leaf carbohydrate dynamics of Pinus edulis during drought-induced tree mortality reveal role for carbon metabolism in mortality mechanism. New Phytol **197**: 1142–1151

Adams HD, Guardiola-Claramonte M, Barron-Gafford GA, Villegas JC, Breshears DD, Zou CB, Troch PA, Huxman TE (2009) Temperature sensitivity of drought-induced tree mortality portends increased regional die-off under global-change-type drought. PNAS **106**: 7063–7066

Adams HD, Zeppel MJB, Anderegg WRL, Hartmann H, Landhausser SM, Tissue DT, Huxman TE, Hudson PJ, Franz TE, Allen CD, et al. (2017b) A multi-species synthesis of physiological mechanisms in drought-induced tree mortality. Nat Ecol Evol **1**: 1285–1291

Aguade D, Poyatos R, Gomez M, Oliva J, Martinez-Vilalta J (2015) The role of defoliation and root rot pathogen infection in driving the mode of drought-related physiological decline in Scots pine (Pinus sylvestris L.). Tree Physiol **35**: 229–242

Bond WJ, Midgley JJ (2003) The evolutionary ecology of sprouting in woody plants. Int J Plant Sci **164**: S103–S114

Breshears DD, Cobb NS, Rich PM, Price KP, Allen CD, Balice RG, Romme WH, Kastens JH, Floyd ML, Belnap J, et al. (2005) Regional vegetation die-off in response to global-change-type drought. PNAS **102**: 15144–15148

Buchanan MK, Oppenheimer M, Kopp RE (2017) Amplification of flood frequencies with local sea level rise and emerging flood regimes. Environ Res Lett **12**: 064009

Cailleret M, Dakos V, Jansen S, Robert EMR, Aakala T, Amoroso MM, Antos JA, Bigler C, Bugmann H, Caccianaga M, et al. (2019) Early-warning signals of individual tree mortality based on annual radial growth. Front Plant Sci **9**: 1964

Camarero JJ, Gazol A, Sangüesa-Barreda G, Oliva J, Vicente-Serrano SM (2015) To die or not to die: early warnings of tree dieback in response to a severe drought. J Ecol **103**: 44–57

Chapin FS, Schulze E-D, Mooney HA (1990) The ecology and economics of storage in plants. Annu Rev Ecol Syst **21**: 423–447

D'Andrea E, Rezaie N, Battistelli A, Gavrichkova O, Kuhlmann I, Matteucci G, Moscatello S, Proietti S, Scartazza A, Trumbore S, et al. (2019) Winter's bite: beech trees survive complete defoliation due to spring late-frost damage by mobilizing old C reserves. New Phytol **224**: 625–631

Desantis LRG, Bhotika S, Williams K, Putz FE (2007) Sea-level rise and drought interactions accelerate forest decline on the Gulf Coast of Florida, USA. Glob Change Biol **13**: 2349–2360

Dickman LT, McDowell NG, Grossiord C, Collins AD, Wolfe BT, Detto M, Wright SJ, Medina-Vega JA, Goodsman D, Rogers A, et al. (2019) Homoeostatic maintenance of nonstructural carbohydrates during the 2015–2016 El Niño drought across a tropical forest precipitation gradient. Plant Cell Environ **42**: 1705–1714

Dickman LT, McDowell NG, Sevanto S, Pangle RE, Pockman WT (2015) Carbohydrate dynamics and mortality in a pinon-juniper woodland under three future precipitation scenarios. Plant Cell Environ **38**: 729–739

Dietze MC, Sala A, Carbone MS, Czimczik CI, Mantooth JA, Richardson AD, Vargas R (2014) Nonstructural Carbon in Woody Plants. Annu Rev Plant Biol **65**: 667–687

Duan H, Chaszar B, Lewis JD, Smith RA, Huxman TE, Tissue DT (2018) CO2 and temperature effects on morphological and physiological traits affecting risk of drought-induced mortality. Tree Physiol **38**: 1138–1151

Fagherazzi S, Anisfeld SC, Blum LK, Long EV, Feagin RA, Fernandes A, Kearney WS, Williams K (2019) Sea Level Rise and the Dynamics of the Marsh-Upland Boundary. Front Environ Sci **7**: 25

Fernandes A, Rollinson CR, Kearney WS, Dietze MC, Fagherazzi S (2018) Declining radial growth response of coastal forests to hurricanes and nor'easters. J Geophys Re Biogeosci **123**: 832–849

Fierravanti A, Rossi S, Kneeshaw D, De Grandpré L, Deslauriers A (2019) Low non-structural carbon accumulation in spring reduces growth and increases mortality in conifers defoliated by spruce budworm. Front For Glob Change **2**: 15

Furze ME, Huggett BA, Aubrecht DM, Stolz CD, Carbone MS, Richardson AD (2019) Whole-tree nonstructural carbohydrate storage and seasonal dynamics in five temperate species. New Phytol **221**: 1466–1477

Galiano L, Martínez-Vilalta J, Lloret F (2011) Carbon reserves and canopy defoliation determine the recovery of Scots pine 4 yr after a drought episode. New Phytol **190**: 750–759

Garcia-Forner N, Sala A, Biel C, Save R, Martinez-Vilalta J (2016) Individual traits as determinants of time to death under extreme drought in Pinus sylvestris L. Tree Physiol **36**: 1196–1209

Gaylord ML, Kolb TE, Pockman WT, Plaut JA, Yepez EA, Macalady AK, Pangle RE, McDowell NG (2013) Drought predisposes pinon-juniper woodlands to insect attacks and mortality. New Phytol **198**: 567–578

Greenway H, Munns R (1980) Mechanisms of salt tolerance in nonhalophytes. Annu Rev Plant Physiol **31**: 149–190

Hammond GE, Lichtner PC, Mills RT (2014) Evaluating the performance of parallel subsurface simulators: an illustrative example with PFLOTRAN. Water Resour Res **50**: 208–228

Hammond WM, Yu K, Wilson LA, Will RE, Anderegg WRL,, Adams HD (2019) Dead or dying? Quantifying the point of no return from hydraulic failure in drought-induced tree mortality. New Phytol **223**: 1834–1843

Harris AS (1990) Picea sitchensis (Bong.) Carr. Sitka spruce. *In* RM Burns, BH Honkala, eds, Silvics of North America, Vol. 1, Conifers. Agricultural Handbook 654. USDA Forest Service, Washington, DC, pp 260–267

Hartmann H, McDowell NG, Trumbore S (2015) Allocation to carbon storage pools in Norway spruce saplings under drought and low CO2. Tree Physiol **35**: 243–252

Hartmann H, Moura CF, Anderegg WRL, Ruehr NK, Salmon Y, Allen CD, Arndt SK, Breshears DD, Davi H, Galbraith D, et al. (2018) Research frontiers for improving our understanding of drought-induced tree and forest mortality. New Phytol **218**: 15–28

Hartmann H, Trumbore S (2016) Understanding the roles of nonstructural carbohydrates in forest trees—from what we can measure to what we want to know. New Phytol **211**: 386–403

Hartmann H, Ziegler W, Kolle O, Trumbore S (2013a) Thirst beats hunger—declining hydration during drought prevents carbon starvation in Norway spruce saplings. New Phytol **200**: 340–349

Hartmann H, Ziegler W, Trumbore S (2013b) Lethal drought leads to reduction in nonstructural carbohydrates in Norway spruce tree roots but not in the canopy. Funct Ecol **27**: 413–427

Hasselquist NJ, Allen MF, Santiago LS (2010) Water relations of evergreen and drought-deciduous trees along a seasonally dry tropical forest chronosequence. Oecologia **164**: 881–890

Hoch G (2015) Carbon reserves as indicators for carbon limitation in trees. Progress in Botany. Springer, Cham, pp 321–346

Huang C, Anderegg WRL, Asner GP (2019) Remote sensing of forest die-off in the Anthropocene: from plant ecophysiology to canopy structure. Remote Sens Environ **231**: 111233

IPCC (2014) Global and sectoral aspects. *In* **Field CB, Barros VR, Dokken DJ, Mach KJ, Mastrandrea MD, Bilir TE, Chatterjee M, Ebi KL, Estrada YO, Genova RC, , et al.** eds, Climate Change 2014: Impacts, Adaptation, and Vulnerability: Part A. Contribution of Working Group II to the Fifth Assessment Report of the Intergovernmental Panel on Climate Change. Cambridge University Press, Cambridge, UK, pp 1–1132

Kemp AC, Horton BP, Donnelly JP, Mann ME, Vermeer M, Rahmstorf S (2011) Climate related sea-level variations over the past two millennia. PNAS **108**: 11017–11022

Kirwan ML, Gedan KB (2019) Sea-level driven land conversion and the formation of ghost forests. Nat Clim Change **9**: 450–457

Kirwan ML, Megonigal JP (2013) Tidal wetland stability in the face of human impacts and sea-level rise. Nature **504**: 53–60

Klein T, Hoch G, Yakir D, Körner C (2014) Drought stress, growth and nonstructural carbohydrate dynamics of pine trees in a semi-arid forest. Tree Physiol **34**: 981–992

Kozlowski TT (1992) Carbohydrate sources and sinks in woody plants. Bot Rev **58**: 107–222

Kozlowski TT (1997) Responses of woody plants to flooding and salinity. Tree Physiol **17**: 490–490

Krauss KW, Noe GB, Duberstein JA, Conner WH, Stagg CL, Cormier N, Jones MC, Bernhardt CE, Lockaby BG, From AS, et al. (2018) The role of the upper tidal estuary in wetland blue carbon storage and flux. Global Biogeochem Cycles **32**: 817–839

Landhäusser SM, Chow PS, Dickman LT, Furze ME, Kuhlman I, Schmid S, Wiesenbauer J, Wild B, Gleixner G, Hartmann H, et al. (2018) Standardized protocols and procedures can precisely and accurately quantify non-structural carbohydrates. Tree Physiol **38**: 1764–1778

LiDAR Bare Earth DEM (2010) Puget Sound LiDAR Consortium. Retrieved from http://pugetsoundlidar.ess.washington.edu/lidardata/restricted/nonpslc/swwash2009/swwash2009.html (accessed November 7, 2019)

Maguire AJ, Kobe RK (2015) Drought and shade deplete nonstructural carbohydrate reserves in seedlings of five temperate tree species. Ecol Evol **5**: 5711–5721

Martínez-Vilalta J, Sala A, Asensio D, Galiano L, Hoch G, Palacio S, Piper FI, Lloret F (2016) Dynamics of non-structural carbohydrates in terrestrial plants: a global synthesis. Ecol Monogr **86**: 495–516

McDowell NG, Allen CD, Anderson-Teixeira K, Brando P, Brienen R, Chambers J, Christoffersen B, Davies S, Doughty C, Duque A, et al. (2018) Drivers and mechanisms of tree mortality in moist tropical forests. New Phytol **219**: 851–869

McDowell NG, Beerling DJ, Breshears DD, Fisher RA, Raffa KF, Stitt M (2011) The interdependence of mechanisms underlying climate-driven vegetation mortality. Trends Ecol Evol **26**: 523–532

McDowell NG, Pockman WT, Allen CD, Breshears DD, Cobb N, Kolb T, Plaut J, Sperry J, West A, Williams DG, et al. (2008) Mechanisms of plant survival and mortality during drought: why do some plants survive while others succumb to drought? New Phytol **178**: 719–739

McDowell NG, Sevanto S (2010) The mechanisms of carbon starvation: how, when, or does it even occur at all? New Phytol **186**: 264–266

Millard P, Sommerkorn M, Grelet G-A (2007) Environmental change and carbon limitation in trees: a biochemical, ecophysiological and ecosystem appraisal. New Phytol **175**: 11–28

Mitchell PJ, O'Grady AP, Tissue DT, Worledge D, Pinkard EA (2014) Co-ordination of growth, gas exchange and hydraulics define the carbon safety margin in tree species with contrasting drought strategies. Tree Physiol **34**: 443–458

Neumann M, Mues V, Moreno A, Hasenauer H, Seidl R (2017) Climate variability drives recent tree mortality in Europe. Glob Chang Biol **23**: 4788–4797

O'Brien MJ, Leuzinger S, Philipson CD, Tay J, Hector A (2014) Drought survival of tropical tree seedlings enhanced by non-structural carbohydrate levels. Nat Clim Change **4**: 710–714

Piper FI, Fajardo A (2016) Carbon dynamics of Acer pseudoplatanus seedlings under drought and complete darkness. Tree Physiol **36**: 1400–1408

Poyatos R, Aguadé D, Galiano L, Mencuccini M, Martínez-Vilalta J (2013) Drought-induced defoliation and long periods of near-zero gas exchange play a key role in accentuating metabolic decline of Scots pine. New Phytol **200**: 388–401

Quentin AG, Pinkard EA, Ryan MG, Tissue DT, Baggett LS, Adams HD, Maillard P, Marchand J, Landhaeusser SM, Lacointe A, et al. (2015) Non-structural carbohydrates in woody plants compared among laboratories. Tree Physiol **35**: 1146–1165

Quirk J, McDowell NG, Leake JR, Hudson PJ, Beerling DJ (2013) increased susceptibility to drought-induced mortality in sequoia sempervirens (cupressaceae) trees under cenozoic atmospheric carbon dioxide starvation. Am J Bot **100**: 582–591

R Core Team (2018) R: A Language and Environment for Statistical Computing. https://www.R-proje ct.org/ (accessed December 10, 2019)

Ross MS, Ogurcak DE, Stoffella S, Sah JP, Hernandez J, Willoughby HE (2019) Hurricanes, storm surge, and pine forest decline on a low limestone island. Estuaries Coast **43**: 1045–1017

Sala A, Piper F, Hoch G (2010) Physiological mechanisms of drought-induced tree mortality are far from being resolved. New Phytol **186**: 274–281

Sapes G, Roskilly B, Dobrowski S, Maneta M, Anderegg WRL, Martinez-Vilalta J, Sala A (2019) Plant water content integrates hydraulics and carbon depletion to predict drought-induced seedling mortality. Tree Physiol **39**: 1300–1312

Sengupta A, Indivero J, Gunn C, Tfaily MM, Chu RK, Toyoda J, Bailey VL, Ward ND, Stegen JC (2019) Spatial gradients in the characteristics of soil-carbon fractions are associated with abiotic features but not microbial communities. Biogeosciences **16**: 3911–3928

Sevanto S, Mcdowell NG, Dickman LT, Pangle R, Pockman WT (2014) How do trees die? A test of the hydraulic failure and carbon starvation hypotheses. Plant Cell Environ **37**: 153–161

Taillie PJ, Moorman CE, Poulter B, Ardón M, Emanuel RE (2019) Decadal-scale vegetation change driven by salinity at leading edge of rising sea level. Ecosystems **22**: 1918–1930

Tattini M, Montagni G, Traversi ML (2002) Gas exchange, water relations and osmotic adjustment in Phillyrea latifolia grown at various salinity concentrations. Tree Physiol **22**: 403–412

Trugman AT, Detto M, Bartlett MK, Medvigy D, Anderegg WRL, Schwalm C, Schaffer B, Pacala SW (2018) Tree carbon allocation explains forest drought-kill and recovery patterns. Ecol Lett **21**: 1552–1560

Wang W, McDowell NG, Ward ND, Indivero J, Gunn C, Bailey VL (2019) Constrained tree growth and gas exchange of seawater-exposed forests in the Pacific Northwest, USA. J Ecol **107**: 2541–2552

Ward ND, Megonigal JP, Bond-Lamberty B, Bailey VL, Butman D, Canuel EA, Diefenderfer H, Ganju NK, Goñi MA, Graham EB, et al. (2020) Representing the function and sensitivity of coastal interfaces in Earth system models. Nature Communications **11**: 2458

Washington Department of Fish and Wildlife (2019) Fish Passage & Diversion Screening Inventory. http://apps.wdfw.wa.gov/fishpassage photos/Reports/980259_Report.pdf (accessed December 10, 2019)

Weber R, Schwendener A, Schmid S, Lambert S, Wiley E, Landhäusser SM, Hartmann H, Hoch G (2018) Living on next to nothing: tree seedlings can survive weeks with very low carbohydrate concentrations. New Phytol **218**: 107–118

Wiley E, Hoch G, Landhäusser SM (2017) Dying piece by piece: carbohydrate dynamics in aspen (Populus tremuloides) seedlings under severe carbon stress. J Exp Bot **68**: 5221–5232

Wiley E, King CM, Landhäusser SM (2019) Identifying the relevant carbohydrate storage pools available for remobilization in aspen roots. Tree Physiol **39**: 1109–1120

Wiley E, Rogers BJ, Hodgkinson R, Landhaeusser SM (2016) Nonstructural carbohydrate dynamics of lodgepole pine dying from mountain pine beetle attack. New Phytol **209**: 550–562

Williams K, Ewel KC, Stumpf RP, Putz FE, Workman TW (1999) Sea-level rise and coastal forest retreat on the West Coast of Florida, USA. Ecology **80**: 2045–2063

Yabusaki SB, Myers-Pigg AN, Ward ND, Waichler SR, Sengupta A, Hou Z, Chen X, Fang Y, Duan Z, Serkowski JA, et al. (2020) Floodplain inundation and salinization from a recently restored first-order tidal stream. Water Resour Res **56**: e2019WR026850